JOURNAL OF MATERIALS SCIENCE 22 (1987) 123–131

Microstructure and superconducting properties of melt-quenched insoluble Al–Pb and Al–Pb–Bi alloys

A. INOUE, N. YANO*, K. MATSUZAKI, T. MASUMOTO
The Research Institute for Iron, Steel and Other Metals, Tohoku University, Sendai 980, Japan

In order to obtain aluminium-based superconducting alloys including finely dispersed lead or Pb–Bi particles, the application of the melt-quenching technique has been tried for Al–Pb, Al–Si–Pb and Al–Si–Pb–Bi alloys containing immiscible elements such as lead and bismuth. It has been found to result in the preparation of superconducting materials consisting of fcc Pb or hcp ε(Pb–Bi) particles dispersed finely and densely in the aluminium-based matrix in each composition range below about 2 at% Pb for Al–Pb alloys and 5 at% Pb or (Pb + Bi) for $(Al_{0.9}Si_{0.1})_{100-x}Pb_x$ and $(Al_{0.9}Si_{0.1})_{100-x}(Pb_{0.6}Bi_{0.4})_x$ alloys. The particle size and interparticle distance were ~40 nm and 40 to 100 nm, respectively, within the grains, and ~100 nm and below ~30 nm, respectively, at the grain boundaries for the lead phase in $Al_{98}Pb_2$ alloy. Particle size was ~15 to 60 nm and interparticle distance 30 to 60 nm for the Pb–Bi phase in $(Al_{0.9}Si_{0.1})_{95}(Pb_{0.6}Bi_{0.4})_5$. Transition temperature, T_c, was 4.16 K for $Al_{98}Pb_2$, 3.94 K for $(Al_{0.9}Si_{0.1})_{95}Pb_5$ and 7.75 K for $(Al_{0.9}Si_{0.1})_{95}(Pb_{0.6}Bi_{0.4})_5$. The upper critical magnetic field, H_{c2}, and critical current density, J_c, for $(Al_{0.9}Si_{0.1})_{95}(Pb_{0.6}Bi_{0.4})_5$ were 0.22 T at 4.2 K and 1.67×10^7 A m^{-2} at zero applied field and 4.2 K. The appearance of the superconductivity for the aluminium-based alloys was interpreted as due to the formation of superconducting percolation path along the tangled dislocations, sub-boundaries and/or grain boundaries where Pb and Pb–Bi phases precipitated preferentially.

1. Introduction

It is well known that the melt-quenching technique leads to many favourable structural modifications of (i) the formation of nonequilibrium crystalline and noncrystalline phases, (ii) the refinement of grain size, (iii) the extension of solid solubility limit, (iv) the suppression of grain boundary segregation, and (v) the suppression of the development of an ordered structure. Additionally, the present authors have very recently demonstrated [1, 2] that the application of the technique to insoluble type alloys is also useful for the achievement of the duplex structure, including homogeneously and finely the second phase which is insoluble in an equilibrium state. For instance, making use of the phenomenon that lead is immiscible into each element of nickel [3], silicon [4], boron [3] and phosphorus [3] in the solid as well as liquid state under an equilibrium condition, the melt-quenching of Ni–Si–B–Pb [5], Ni–P–B–Pb [5], Cu–Ni–P–Pb [6], Fe–P–Pb [7] and Co–Si–B–Pb [7] alloys has been reported to form a duplex structure consisting of an amorphous matrix phase and fine lead particles. Furthermore, the duplex alloys have been found to exhibit superconductivity by the proximity effect of the superconducting lead particles, even though the nickel-, copper-, iron- and cobalt-based amorphous phases themselves are nonsuperconductive.

Similarly, for the Al–Pb alloy containing lead above about 0.2 at %, both the elements are insoluble in liquid and solid states [3], and hence it is very difficult to obtain the duplex aluminium-based alloy with a finely and uniformly dispersed lead phase by the conventional solidification technique. However, if the duplex structure with finely dispersed immiscible particles can be obtained for Al–Pb alloys by the melt-quenching technique, the aluminium-based alloys are highly attractive as a soft-type superconductor combined with high electrical conductivity and high ductility. This paper intends

1. to clarify the features of the microstructure of melt-quenched Al–Pb, Al–Si–Pb and Al–Si–Pb–Bi alloys, and the maximum lead and lead plus bismuth contents at which the aluminium alloys with finely and uniformly dispersed lead and lead plus bismuth particles can be obtained;
2. to examine whether or not the duplex alloys exhibit a superconductivity by the dispersion of the lead and lead plus bismuth particles;
3. to investigate the features of the superconductivity of the melt-quenched Al–Pb, Al–Si–Pb and Al–Si–Pb–Bi alloys by comparing the present results with the previously reported superconductivity of the nickel- and copper-based alloys which was achieved

Permanent address: Unitika Research and Development Center, Unitika Ltd, Uji 611, Japan.

0022–2461/87 $03.00 + .12

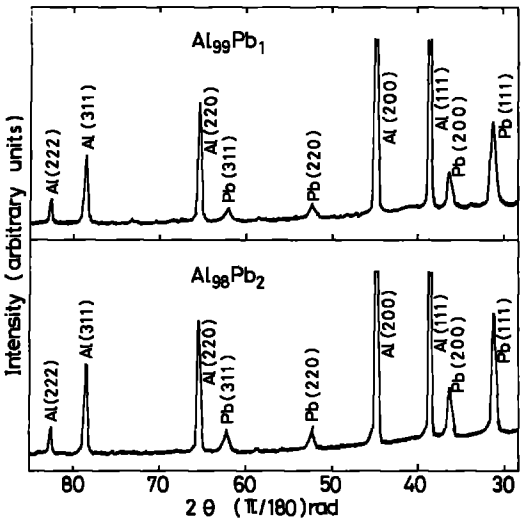

Figure 1 X-ray diffraction patterns showing the duplex structure consisting of fcc aluminium and fcc lead phases in melt-quenched (a) $Al_{99}Pb_1$ and (b) $Al_{98}Pb_2$ alloys.

by the dispersion of lead and lead plus bismuth particles in the amorphous phase with an extremely short mean free path of electrons.

2. Experimental procedure

$Al_{100-x}Pb_x$, $(Al_{0.9}Si_{0.1})_{100-x}Pb_x$, and $(Al_{0.9}Si_{0.1})_{100-x}(Pb_{0.6}Bi_{0.4})_x$ ($x \leqslant 10$ at %) alloys with different compositions were prealloyed under a purified and gettered argon atmosphere in an arc furnace from pure elements of aluminium (99.9 wt %), lead (99.9 wt %), silicon (99.999 wt %) and bismuth (99.99 wt %). Typically, the amount of each ingot in one arc melting was about 2 g, and the whole ingot was used in one melt-quenching operation to produce ribbon samples of about 2 mm width and 0.02 mm thickness in air by a single-roller spinning apparatus with a copper wheel. The compositions of the alloys are nominal, since the loss of lead content during arc melting was less than about 0.4 wt %. The as-quenched structure was examined by X-ray diffractometry and optical, scanning and transmission electron microscopies.

All measurements of superconducting and electrical properties, transition temperature, T_c, critical current density, $J_c(H)$, upper critical magnetic field, $H_{c2}(T)$, flux flow resistivity, $\varrho_f(H)$, and electrical resistivity, $\varrho(T)$, were made using a conventional DC four-probe technique. The critical current was defined as the threshold current at which no zero voltage ($> 1\,\mu V$) was first detected. The magnetic field up to 9 T was applied transversely to the specimen surface and feed current. The temperature was measured using a calibrated germanium thermometer at temperatures below about 90 K and a calibrated diode thermometer in the higher temperature range with accuracy better than ± 0.01 K at temperatures below 90 K and ± 0.1 K at the higher temperatures.

3. Results

3.1. Melt-quenched structure

Fig. 1 shows the X-ray diffraction patterns of melt-quenched $Al_{99}Pb_1$ and $Al_{98}Pb_2$ alloys. Some weak diffraction peaks corresponding to fcc lead are seen in addition to the diffraction peaks of fcc aluminium with high intensities, indicating the formation of a coexistent structure of aluminium and lead. Additionally, it is seen that the intensity of the diffraction peaks from lead increases continuously with increasing lead content from 1 to 2 at %. The increase in additional lead content appears to result in an increase in precipitation amount rather than an increase in the amount of dissolved lead in the aluminium matrix phase. The lattice parameters of lead and aluminium are, respectively, 0.4951 nm and 0.4048 nm for $Al_{99}Pb_1$ and 0.4954 nm and 0.4050 nm for $Al_{98}Pb_2$. These values are nearly the same as those (0.49502 nm and 0.40496 nm) [8] for pure lead and aluminium and no systematic variation in their lattice parameters with lead content is seen, indicating that both the metals are almost completely insoluble with each other in the rapidly solidified state, as is expected from the equilibrium phase diagram of Al–Pb [2].

Fig. 2 shows the typical transmission electron micrographs revealing the distribution of lead particles in a melt-quenched $Al_{98}Pb_2$ alloy. As seen in the photographs, the distribution of lead particles is very uniform within the grains except the region near the grain boundaries, where the precipitation free zone (PFZ) appears by a preferential precipitation of lead on the grain boundaries of aluminium. The average grain size (D) of the aluminium matrix is about 1.2 μm and the width of the PFZ is measured to be about

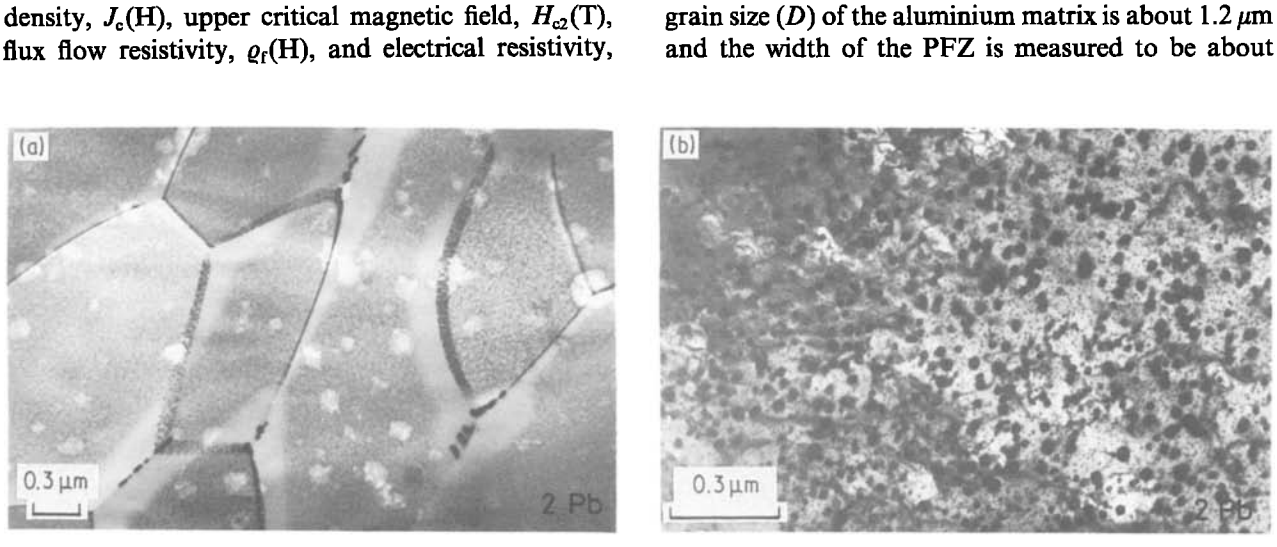

Figure 2 Transmission electron micrographs showing the duplex structure consisting of finely dispersed fcc lead particles in aluminium matrix for a melt-quenched $Al_{98}Pb_2$ alloy.

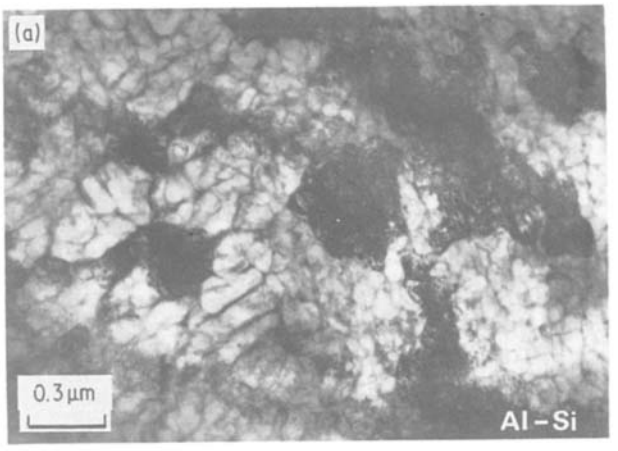

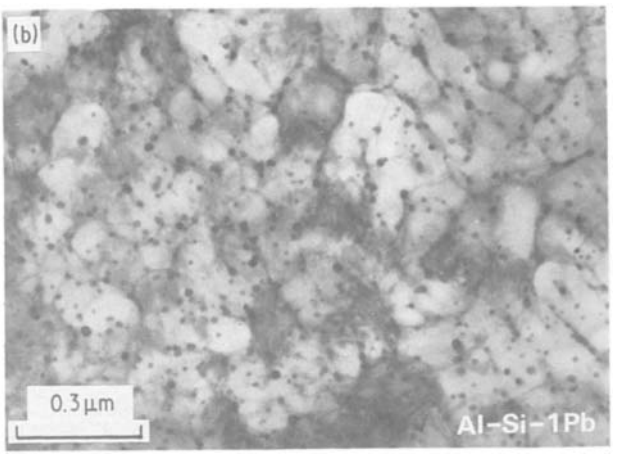

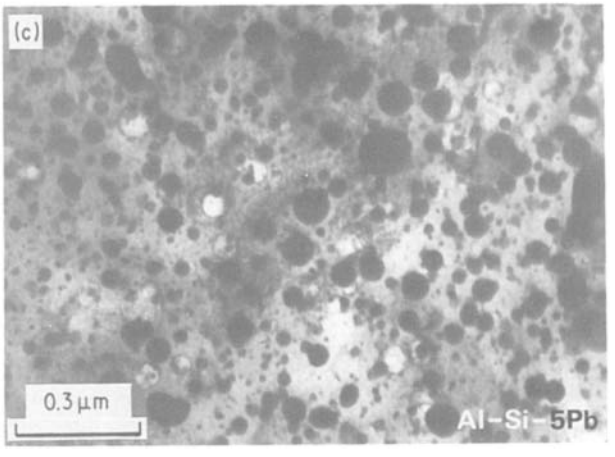

Figure 3 Transmission electron micrographs showing (a) the fcc Al(Si) single phase in a melt-quenched $Al_{90}Si_{10}$ alloy, and the duplex phases consisting of finely dispersed lead particles in Al(Si) matrix for melt-quenched (b) $(Al_{0.9}Si_{0.1})_{99}Pb_1$ and (c) $(Al_{0.9}Si_{0.1})_{95}Pb_5$ alloys.

0.2*D*. The average diameter and the interparticle distance of lead particles are estimated to be ~40 nm and 40 to 100 nm, respectively, within the grains, and ~100 nm and below ~30 nm, respectively, at the grain boundaries. Thus the growth of lead particles is much easier at the grain boundaries than within the grains due to a greater diffusivity of the solute element. Additionally, Fig. 2b shows the size of the lead particles roughly divided into two groups: ~40 nm and ~4 nm. Although the reason for such a clearly distinguishable difference in particle size is not clear, it may be due to the difference in precipitation temperature resulting from the difference in the precipitation process. That is, the larger particles appear directly from liquidus lead at a realtively high temperature, while the finer particles precipitate from the supersaturated aluminium solid solution at a rather low temperature upon self-annealing during cooling after solidification was complete. Additionally, the existence of the PFZ strongly supports the possibility that the fine lead particles precipitate from the aluminium solid solution. It is important to point out that the increase to 3 at % in the additional amount of lead resulted in the formation of macroscopically phase-separated ribbon samples consisting of a pure lead region and an aluminium-based region including fine lead particles, and hence the formation of the Al–Pb alloys with uniformly dispersed lead particles was limited to less than ~2 at % Pb (about 13.6 wt % Pb).

The formation of the PFZ and the two distinct groups of lead particle size indicate that the melt quenching of Al–Pb binary alloys during and after solidification is not rapid enough to achieve a completely homogeneous duplex structure. Accordingly, in the subsequent investigation, the effect of the addition of a silicon element (which has been reported [9] to be very effective in enhancing the supercooling ability of aluminium-based alloys) to the melt-quenched structure of Al–Pb alloys, was examined with the aim of obtaining the duplex structure including lead particles with a more uniform size. Fig. 3 shows transmission electron micrographs of melt-quenched $Al_{90}Si_{10}$, $(Al_{0.9}Si_{0.1})_{98}Pb_2$ and $(Al_{0.9}Si_{0.1})_{95}Pb_5$ alloys. As is evident from the comparison between Figs 2 and 3, the addition of silicon results in a more uniform distribution of lead particles through the suppression of the formation of the PFZ and the homogenization of the lead particle size, which is caused by the suppression of the precipitation upon self-annealing after solidification was complete. The structural change indicates the achievement of the duplex structure including finely and uniformly dispersed lead particles in the aluminium-based matrix through the enhancement of the supercooling ability of the molten alloy. The lattice parameters of the Al(Si) matrix and the lead particles determined from the X-ray analysis are 0.4042 and 0.4953 nm, respectively, for the Al–Si–5Pb alloy. From the linear extrapolation of the previously reported lattice parameters of Al(Si) solid solution containing less than 0.93 at % Si [8], the Al(Si) matrix is estimated to contain about 8.7 at % Si, in accordance with the nominal silicon concentration of the alloy.

The partial replacement of the lead by bismuth for $(Al_{0.9}Si_{0.1})_{100-x}Pb_x$ (x = 5 at %) alloys results in a change of the as-quenched structure from fcc Al(Si) and fcc lead to a mixed structure consisting of Al(Si), hcp ε(Pb–Bi) with $a \simeq 0.351$ nm and $c \simeq 0.580$ nm, bct X phase with $a \simeq 0.993$ nm and $c \simeq 1.449$ m, and hexagonal bismuth with $a \simeq 0.455$ nm and $c \simeq 1.186$ nm. The particle size of the precipitates decreases significantly from about 100 nm for $(Al_{0.9}Si_{0.1})_{95}Pb_5$ to about 40 nm for

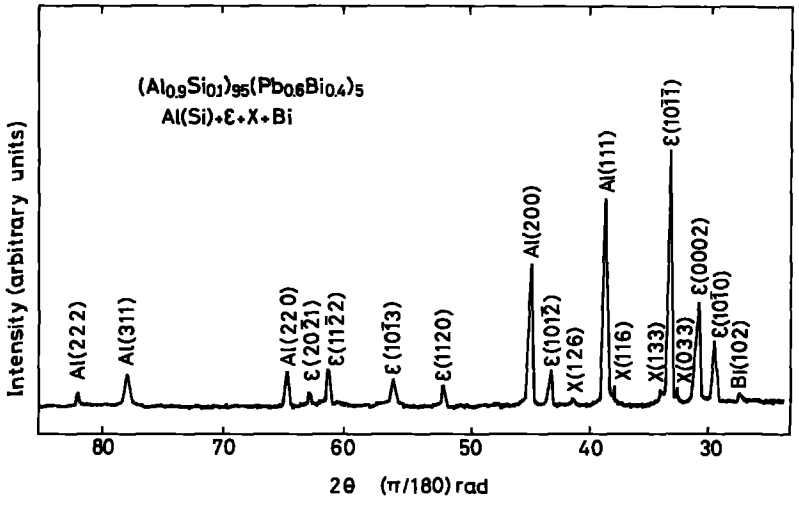

Figure 4 X-ray diffraction pattern showing the duplex structure consisting of fcc Al(Si) and hcp ε(Pb–Bi) phases in a melt-quenched $(Al_{0.9}Si_{0.1})_{95}Pb_3Bi_2$ alloy.

$(Al_{0.9}Si_{0.1})_{95}Pb_3Bi_2$, as exemplified by the X-ray diffraction pattern and transmission electron micrograph in Figs 4 and 5. The ε phase is a supersaturated solid solution of the equilibrium hcp phase which exists in the range 24 to 33 at % Bi at room temperature [10, 11], and the *X* phase is a nonequilibrium phase which appears only in the rapidly solidified case [12]. From the X-ray diffraction intensities of ε(Pb–Bi), *X* and Bi phases shown in Fig. 4, the precipitates are concluded to be mainly composed of the ε(Pb–Bi) phase.

3.2. Superconducting properties

Fig. 6 shows typical examples of the normalized electrical resistance (R/R_n) curves in the vicinity of T_c in the case of no applied magnetic field for (a) $Al_{100-x}Pb_x$ (x = 1 and 2 at %) and (b) $(Al_{0.9}Si_{0.1})_{100-x}Pb_x$ (x = 1, 2 and 5 at %) alloys. Here R_n is the resistance in the normal state. The transition occurs rather broadly with a temperature width (ΔT_c) of 0.72 to 0.86 K for the Al–Pb alloys and from 1.20 to 2.05 K for the Al–Si–Pb alloys. The transition temperature, T_c, which was taken as the temperature at R/R_n = 0.5, is 3.10 K at 1% Pb and 4.16 K at 2% Pb for $Al_{100-x}Pb_x$ alloys and 2.54 K at 1% Pb, 2.94 K at 2% Pb and 3.94 K at 5% Pb for $(Al_{0.9}Si_{0.1})_{100-x}Pb_x$ alloys. Additionally, Fig. 7 shows the change in T_c as a function of lead or silicon content for Al–Pb and Al–Si–Pb alloys. Whilst T_c rises continuously with increasing lead content, the addition of silicon reduces T_c. T_c of the alloys containing the same lead content is lower for the Al–Si–Pb system than for the Al–Pb system. The reason for the difference in T_c between Al–Pb and Al–Si–Pb alloys is discussed below on the basis of the size and interparticle distance of lead particles.

In order to obtain the aluminium-based alloys exhibiting a high T_c value, the effect on T_c of the replacement of lead by *M*, where *M* is bismuth, tin or antimony, was examined for the series of $(Al_{0.9}Si_{0.1})_{98}(Pb_{1-x}M_x)_2$ alloys in which the formation of a ribbon sample is much easier as compared with $Al_{98}Pb_2$ alloy. The normalized electrical resistance curves of the Al–Si–2(Pb–*M*) alloys presented in Fig. 8 show that $(Al_{0.9}Si_{0.1})_{98}(Pb_{0.6}Bi_{0.4})_2$ exhibits the highest T_c of 7.38 K as well as a rather small ΔT_c of 0.76 K. Additionally, Fig. 8 shows that the increase of

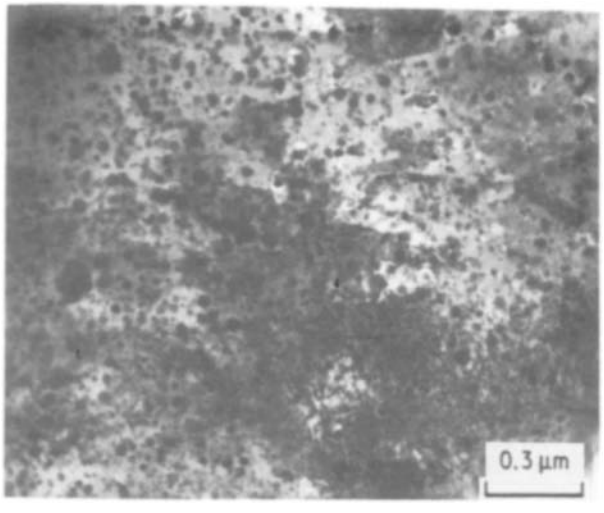

Figure 5 Transmission electron micrograph showing the duplex structure consisting of finely dispersed ε(Pb–Bi) particles in Al(Si) matrix for a melt-quenched $(Al_{0.9}Si_{0.1})_{95}Pb_3Bi_2$ alloy.

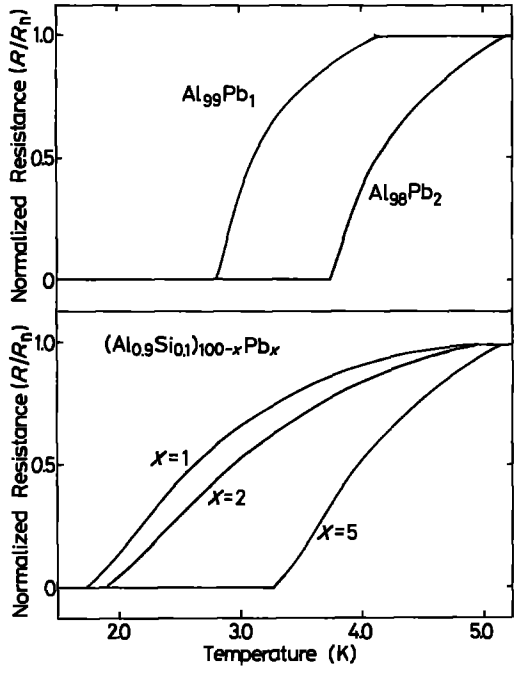

Figure 6 Normalized resistance ratio R/R_n as a function of temperature for melt-quenched (a) $Al_{100-x}Pb_x$ (x = 1 and 2 at %) and (b) $(Al_{0.9}Si_{0.1})_{100-x}Pb_x$ (x = 1, 2 and 5 at %) alloys possessing the coexistent fcc lead and fcc aluminium or fcc Al(Si) phases.

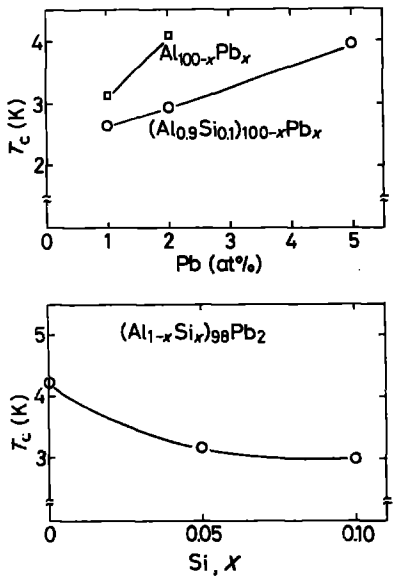

Figure 7 Changes in T_c as a function of lead or silicon content for melt-quenched (a) $Al_{100-x}Pb_x$ (x = 1 and 2 at%) and $(Al_{0.9}Si_{0.1})_{100-x}Pb_x$ (x = 1, 2 and 5 at%) and (b) $(Al\text{–}Si)_{98}Pb_2$ alloys possessing the coexistent fcc lead and fcc aluminium or fcc Al(Si) phases.

lead plus bismuth content into 5 at% results in a further rise of T_c into 7.75 K. However, the highest T_c value is lower by about 1.1 K than the highest value (8.9 K) [13] of the bulky Pb–Bi alloy reported previously. No aluminium-based superconducting alloys exhibiting the same value as the highest T_c value of $Pb_{60}Bi_{40}$ were obtained within the present investigation, even though the duplex phases consisting of amorphous and ε(Pb + Bi) phases in Ni–Si(or P)–B–Pb–Bi [5] and Cu–Ni–P–Pb–Bi [6] alloys exhibit a high T_c of 8.9 K, which is equal to the highest T_c value of $Pb_{60}Bi_{40}$.

The upper critical magnetic field, H_{c2}, was measured at various temperatures ranging from 4.2 K to T_c for $(Al_{0.9}Si_{0.1})_{98}(Pb_{0.6}Bi_{0.4})_2$ and $(Al_{0.9}Si_{0.1})_{95}(Pb_{0.6}Bi_{0.4})_5$ alloys exhibiting high T_c. As an example, Fig. 9 shows the transition curves from the superconducting state to the normal state for $(Al_{0.9}Si_{0.1})_{95}(Pb_{0.6}Bi_{0.4})_5$ at different temperatures under a current density of 1.8×10^4 A m^{-2}. Resistive states are limited to a relatively narrow range of fields, and the range decreases from 0.23 to 0.05 T with a temperature rise from 4.29 to 7.50 K. Here we define H_{c2} to be the applied magnetic field at which the resistance of the sample begins to appear. The temperature dependence of H_{c2} for $(Al_{0.9}Si_{0.1})_{98}(Pb_{0.6}Bi_{0.4})_2$ and $(Al_{0.9}Si_{0.1})_{95}(Pb_{0.6}Bi_{0.4})_5$ alloys is shown in Fig. 10, where the solid line represents a linear extrapolation near T_c. The H_{c2} increases linearly with decreasing temperature in the temperature range below $t = T/T_c \simeq 0.7$, and the gradient near T_c, $-(dH_{c2}/dT)_{T_c}$, is 0.07 T K^{-1} for the former alloy and 0.075 T K^{-1} for the latter alloy. The H_{c2} at 4.2 K is 0.196 T for the Al–Si–2(Pb–Bi) alloy and 0.212 T for the Al–Si–5(Pb–Bi) alloy. Thus, the H_{c2} and $-(dH_{c2}/dT)_{T_c}$ as well as T_c are higher for the alloy containing a larger amount of lead and bismuth.

The critical current density, J_c, for $(Al_{0.9}Si_{0.1})_{98}$-$(Pb_{0.6}Bi_{0.4})_2$ and $(Al_{0.9}Si_{0.1})_{95}(Pb_{0.6}Bi_{0.4})_5$ alloys was measured at 4.2 K under an external applied magnetic field. The J_c values as a function of external applied field are plotted in Fig. 11. Additionally, the fluxoid pinning force, F_p, evaluated from Fig. 11 is plotted as a function of reduced magnetic field H/H_{c2} in Fig. 12, where F_p is calculated as $J_c \times H$. The maximum F_p at 4.2 K and the value of H/H_{c2} where F_p shows a maximum are, respectively, 1.8×10^5 N m^{-3} and 0.15 for the Al–Si–2(Pb–Bi) alloy and 8.2×10^5 N m^{-3} and 0.25 for the Al–Si–5(Pb–Bi) alloy.

4. Discussion

4.1. Features of the dispersed state of lead and ε(Pb–Bi) particles in aluminium-based alloys

The particle size ($2r$) and interparticle distance (D) of lead and ε(Pb–Bi) particles in melt-quenched $Al_{100-x}Pb_x$ (x = 1 and 2 at%), $(Al_{0.9}Si_{0.1})_{100-x}Pb_x$ (x = 1, 2 and 5 at%) and $(Al_{0.9}Si_{0.1})_{100-x}(Pb_{0.6}Bi_{0.4})_x$ (x = 2 and 5 at%) alloys are summarized in Table I. The data of nickel- [5] and copper- [6] based amorphous alloys including immiscible lead and lead–bismuth particles are also shown for comparison. As shown in Table I, the $2r$ and D values for the aluminium-based crystalline matrix are in the range of 5 to 50 nm and 40 to 100 nm, respectively, and their values are smaller by a factor of about 4 to 600 and 2 to 88, respectively, than those for the nickel- and copper-based amorphous alloys. Thus, the dispersion of insoluble lead and lead–bismuth particles in melt-quenched aluminium-based alloys is concluded to be in a very fine state. The achievement of such a fine duplex structure is interpreted as due to the simultaneous satisfaction of the following two factors.

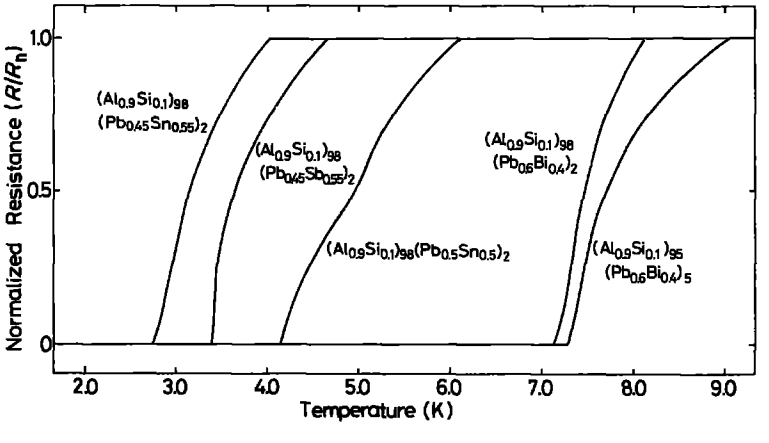

Figure 8 Normalized resistance ratio R/R_n as a function of temperature for melt-quenched $(Al_{0.9}$-$Si_{0.1})_{98}(Pb_{0.6}Bi_{0.4})_2$, $(Al_{0.9}Si_{0.1})_{95}(Pb_{0.6}Bi_{0.4})_5$, $(Al_{0.9}$-$Si_{0.1})_{98}(Pb_{0.45}Sb_{0.55})_2$ and $(Al_{0.9}Si_{0.1})_{98}(Pb_{0.5}Sn_{0.5})_2$ alloys possessing the coexistent fcc Al(Si) and hcp ε(Pb–Bi).

TABLE I Particle size, $2r$, and interparticle distance, D, of fcc lead and hcp ε(Pb–Bi) phases embedded in aluminium matrix, for melt-quenched aluminium-based alloys. Data for melt-quenched nickel- and copper-based alloys with the duplex structure of amorphous and lead or ε(Pb–Bi) phases [5, 6] are also presented for comparison

Alloy (at %)	$2r$ (nm)	D (nm)	T_c (K)	ΔT_c (K)	$-(dH_{c2}/dT)_{T_c}$ (T/K)	H_{c2} at 4.2 K (T)	ϱ_n ($\mu\Omega$m)	r/ξ_0^*
$Al_{99}Pb_1$	10–20	20–30	3.10	0.70	–	–	0.0011	0.06–0.12
$Al_{98}Pb_2$	40	40–100	4.16	0.85	–	–	0.0027	0.24
$(Al_{0.9}Si_{0.1})_{99}Pb_1$	10	15–40	2.54	1.85	–	–	–	0.06
$(Al_{0.9}Si_{0.1})_{98}Pb_2$	40	30–100	2.94	2.15	–	–	–	0.24
$(Al_{0.9}Si_{0.1})_{95}Pb_5$	100	50–120	3.94	1.19	–	–	–	0.60
$(Al_{0.9}Si_{0.1})_{98}Pb_{1.2}Bi_{0.8}$	20–40	20–70	7.38	0.76	0.070	0.196	0.14	0.43–0.87
$(Al_{0.9}Si_{0.1})_{95}Pb_3Bi_2$	15–60	30–60	7.75	1.10	0.075	0.212	0.16	0.33–1.30
$(Ni_{0.8}P_{0.1}B_{0.1})_{95}Pb_5$ [5]	1000–1500	800–1500	7.5	0.55	5.99×10^{-3}	0.46	0.64	6–9
$(Ni_{0.75}Si_{0.08}B_{0.17})_{95}Pb_5$ [5]	1500–3000	2500–3500	7.1	0.73	–	–	0.17	9–18
$(Ni_{0.8}P_{0.1}B_{0.1})_{95}Pb_3Bi_2$ [5]	–	–	8.8	0.18	0.32	1.40	2.00	–
$(Ni_{0.75}Si_{0.08}B_{0.17})_{95}Pb_3Bi_2$ [5]	200–500	200–700	8.6	0.35	0.35	1.60	1.70	4–11
$(Cu_{0.65}Ni_{0.18}P_{0.17})_{95}Pb_5$ [6]	300–1500	500–2000	6.9	0.56	–	–	0.30	2–9
$(Cu_{0.65}Ni_{0.18}P_{0.17})_{95}Pb_3Bi_2$ [6]	500–700	800–1000	8.7	0.52	0.34	1.55	1.73	11–15

1. The melting temperature of the base metal is the lowest for aluminium. Accordingly, the difference of melting temperature between their alloys and lead or Pb_3Bi_2 is much smaller for aluminium-based alloys, leading to the suppression of the coalescence and growth of lead particles during cooling after solidification.

2. The melt-quenched crystalline aluminium alloys contain a high density of grain boundaries, sub-boundaries, dislocations and point defects which act as preferential precipitation sites of insoluble lead or lead–bismuth particles, leading to the formation of a finer dispersed structure. On the contrary, a relatively coarse dispersion of lead and lead–bismuth particles for the nickel- [5] and copper- [6] based amorphous alloys is interpreted as due to the high melting temperature of the nickel- and copper-based alloys and a very homogeneous structure without grain boundaries and sub-boundaries which are effective for the nucleation site of the immiscible metal particles.

4.2. Mechanism for the appearance of superconductivity for aluminium-based alloys including lead and lead–bismuth particles

It is well known [13] that the aluminium and Al–Si crystalline alloys do not exhibit superconductivity at temperatures above 1.5 K under a conventional atmospheric pressure. Accordingly, as a mechanism for the superconductivity of the duplex alloys, one may propose the following three concepts, i.e. (i) the formation of a surface thin layer of superconducting lead or lead–bismuth phase, (ii) the formation of percolation path of lead or lead–bismuth, and (iii) the proximity effect due to lead or lead–bismuth particles. Judging from the result that the superconductivity presented above remains almost unchanged, even after the 20% reduction in the ribbon thickness, by any method of chemical, electrical or mechanical polishing, it is unreasonable to assume the existence of the superconducting path by the surface thin layer.

Secondarily, we shall consider the case where the present appearance of superconductivity for the aluminium-based alloys is due to the proximity effect which results from the lead or lead–bismuth superconducting particles embedded in isolation in the aluminium matrix. The residual electrical resistivity (ϱ_n) of melt-quenched pure aluminium and $Al_{90}Si_{10}$ alloys was measured to be about 3.7×10^{-4} and 0.115 $\mu\Omega$ m, respectively. From the ϱ_n values, the mean free path of electron (l) is estimated to be about 1.1×10^5 nm for aluminium and about 350 nm for $Al_{90}Si_{10}$ from the nearly free electron model [14]. Further, the coherence length (ξ_0) at 0 K for a pure aluminium superconductor has been reported to be of the order of 1600 nm [15] and the ξ_0 value of an Al(Si) superconductor is roughly estimated to be of the order of 100 nm from the Pippard relation of $\xi_0 = 0.15(h v_F/$

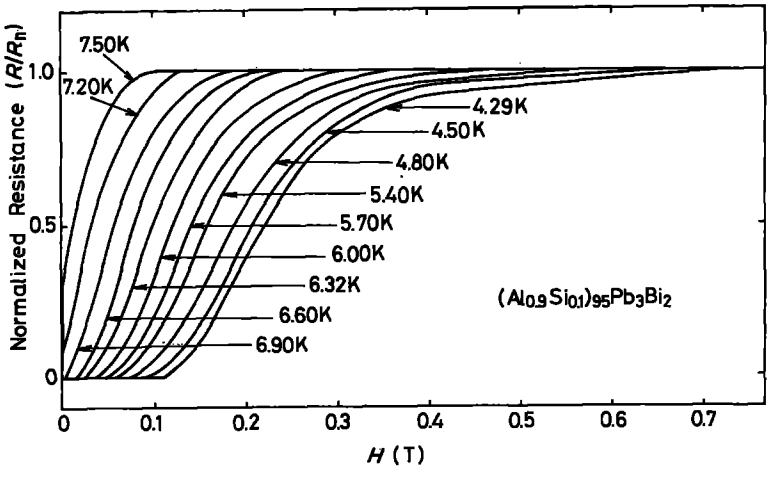

Figure 9 Normalized resistance ratio R/R_n as a function of magnetic field at various temperatures for a melt-quenched $(Al_{0.9}Si_{0.1})_{95}(Pb_{0.6}Bi_{0.4})_5$ alloy possessing the coexistent hcp ε(Pb–Bi) and fcc Al(Si) phases.

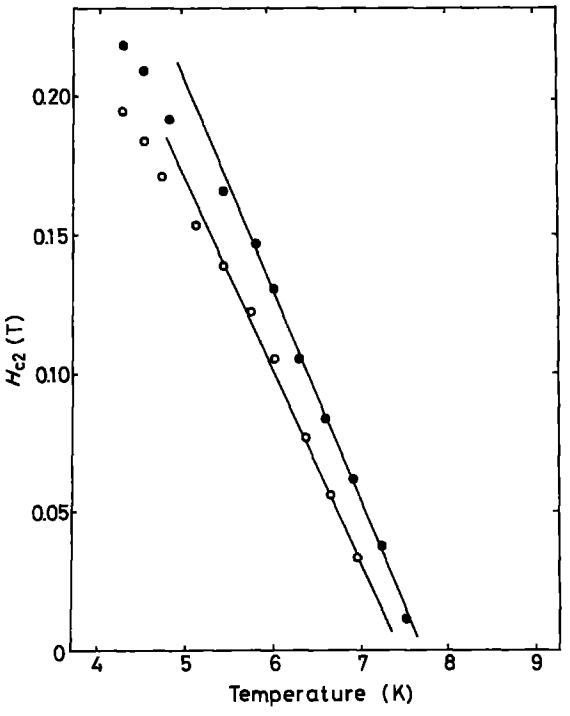

Figure 10 The upper critical magnetic field (H_{c2}) as a function of temperature for a melt-quenched $(Al_{0.9}Si_{0.1})_{98}(Pb_{0.6}Bi_{0.4})_2$ and $(Al_{0.9}Si_{0.1})_{95}(Pb_{0.6}Bi_{0.4})_5$ alloys possessing the coexistent hcp ε(Pb–Bi) and fcc Al(Si) phases. ○, $(Al_{0.9}Si_{0.1})_{98}(Pb_{0.6}Bi_{0.4})_2$ – $(dH_{c2}/dT)_{T_c} = 0.070$ T/K; ●, $(Al_{0.9}Si_{0.1})_{95}(Pb_{0.6}Bi_{0.4})_5$ – $(dH_{c2}/dT)_{T_c} = 0.075$ T/K.

$k_B T_c$) [16]. Here v_F is the Fermi velocity of electrons in the Al(Si) alloy. Since the degree of appearance of superconductivity by the proximity effect has been considered to be dominated by the characteristics of the matrix phase [17], the present alloys consisting of aluminium or aluminium(silicon) and lead or lead–bismuth phases can therefore be classified as a clean type superconductor because $l \geqslant \xi_0$ for the crystalline aluminium and Al(Si) matrix.

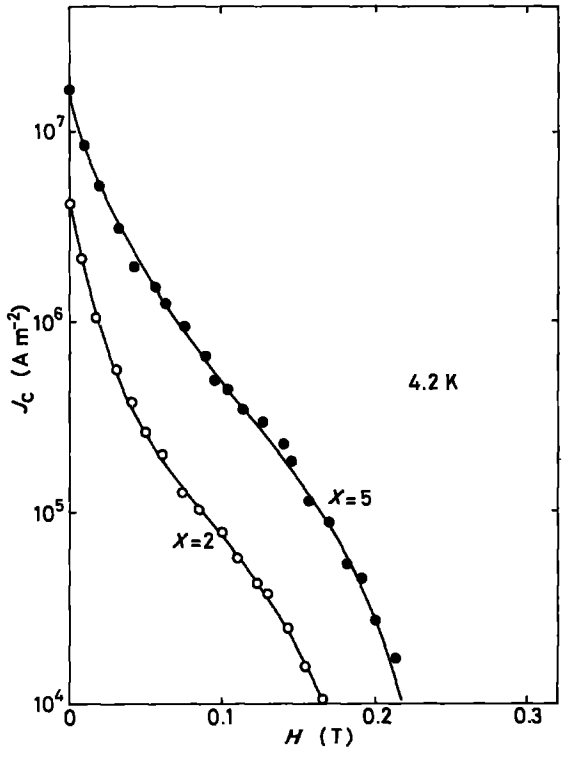

Figure 11 Critical current density, J_c, as a function of magnetic field for melt-quenched $(Al_{0.9}Si_{0.1})_{98}(Pb_{0.6}Bi_{0.4})_2$ and $(Al_{0.9}Si_{0.1})_{95}(Pb_{0.6}Bi_{0.4})_5$ alloys possessing the coexistent hcp ε(Pb–Bi) and fcc Al(Si) phases.

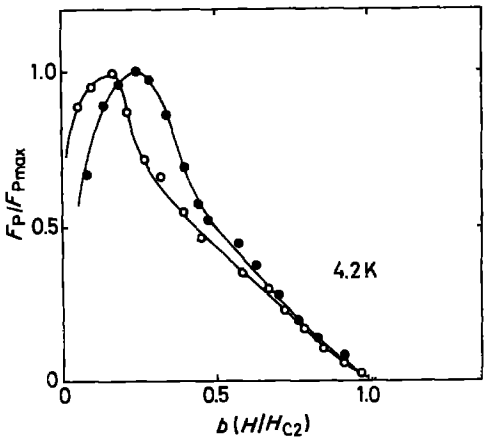

Figure 12 Fluxoid pinning force F_p as a function of reduced magnetic field H/H_{c2} for a melt-quenched $(Al_{0.9}Si_{0.1})_{98}(Pb_{0.6}Bi_{0.4})_2$ and $(Al_{0.9}Si_{0.1})_{95}(Pb_{0.6}Bi_{0.4})_5$ alloys possessing the coexistent hcp ε(Pb–Bi) and fcc Al(Si) phases. ○, $(Al_{0.9}Si_{0.1})_{98}(Pb_{0.6}Bi_{0.4})_2$, $F_{Pmax} = 1.8 \times 10^5$ N m^3; ●, $(Al_{0.9}Si_{0.1})_{95}(Pb_{0.6}Bi_{0.4})_5$, $F_{Pmax} = 8.2 \times 10^5$ N m^3.

For the proximity effect in the case of clean limit, the leak distance (K_n^{-1}) is given by [17],

$$K_n^{-1} = h v_n / 2\pi k_B T \quad (1)$$

Here v_n is the Fermi velocity of electrons in normal conducting aluminium alloy. The above equation indicates that K_n^{-1} is influenced only by the electron in normal conducting matrix phase. K_n^{-1} for the aluminium matrix phase is estimated to be about 2.2×10^3 nm by using the v_n value (2.02×10^6 msec^{-1}) [15] of pure aluminium. The K_n^{-1} value is rather large and the interparticle distance of the superconducting lead and lead–bismuth particles in the aluminium matrix for exhibiting a high T_c by the proximity effect is required to be less than 4.4×10^3 nm. As seen in Table I which summarizes the superconducting and electrical properties, the criterion of the lead distance is completely satisfied for all the aluminium-based alloys including lead or lead–bismuth particles.

Additionally, in order to achieve a superconductivity exhibiting the same T_c as that of the superconducting particles, the critical radius of superconducting lead or lead–bismuth particles (r_c) for the proximity effect in the case of $L = l/\xi = 1$ must be above $2.965\xi_0^*$ [18], where ξ is the BCS coherence length of the aluminium matrix phase, and ξ_0^* is the coherence length of lead or lead–bismuth particles. The ξ_0^* value has been reported to be 83 nm for pure lead [15] and 23 nm for $Pb_{80}Bi_{20}$ [19]. As a result, r_c is estimated to be about 250 nm for lead and about 70 nm for $Pb_{60}Bi_{40}$, if one assumes that the ξ_0^* value of $Pb_{60}Bi_{40}$ particles is nearly the same as that of $Pb_{80}Bi_{20}$ alloy. This estimation indicates that the radius of lead and $Pb_{60}Bi_{40}$ particles must be larger than about 250 and 70 nm, respectively, in the case of $L = l/\xi = 1$ for achieving high T_c values by the proximity effect, in addition to the criterion of the leak distance. As summarized in Table I, the particle radius of lead and

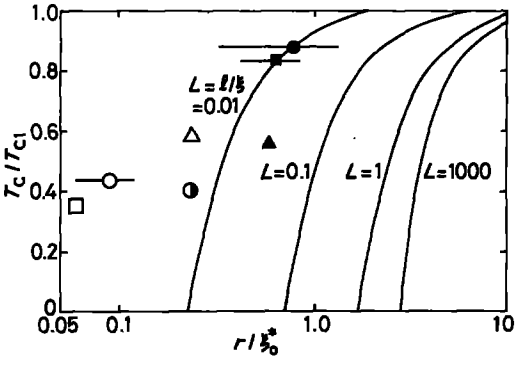

Figure 13 Theoretically estimated T_c/T_{c1} values as a function of r/ξ_0^* for melt-quenched $Al_{99}Pb_1$, $Al_{98}Pb_2$, $(Al_{0.9}Si_{0.1})_{100-x}Pb_{x1}$ (x = 1, 2 and 5 at %) and $(Al_{0.9}Si_{0.1})_{100-x}(Pb_{0.6}Bi_{0.4})_x$ (x = 2 and 5 at %) alloys possessing the coexistent fcc lead and fcc aluminium or fcc Al(Si) phases. Average r/ξ_0^* values: ○, $Al_{99}Pb_1$; △, $Al_{98}Pb_2$; □, $(Al_{0.9}Si_{0.1})_{99}Pb_1$; ◑, $(Al_{0.9}Si_{0.1})_{98}Pb_2$; ▲, $(Al_{0.9}Si_{0.1})_{95}Pb_5$; ■, $(Al_{0.9}Si_{0.1})_{98}Pb_{1.2}Bi_{0.8}$; ●, $(Al_{0.9}Si_{0.1})_{95}Pb_3Bi_2$.

$Pb_{60}Bi_{40}$ phase is about 0.02 to 0.04 r_c for $Al_{99}Pb_1$, about 0.08 r_c for $Al_{98}Pb_2$, about 0.02 r_c for $(Al_{0.9}Si_{0.1})_{95}Pb_5$, 0.14 to 0.29 r_c for $(Al_{0.9}Si_{0.1})_{98}(Pb_{0.6}Bi_{0.4})_2$ and 0.11 to 0.43 r_c for $(Al_{0.9}Si_{0.1})_{95}(Pb_{0.6}Bi_{0.4})_5$. Furthermore, the actual value of $L = l/\xi$ for the present superconductor is greater than one, and is estimated to be about 70 for the Al–Pb alloy, and 1 to 10 for the Al–Si–Pb–Bi alloys. The theoretical analyses [20, 21] on the variation of normalized transition temperature (T_c/T_{c1}) of the duplex alloys as a function of r/ξ_0^* have been given in the cases of different l/ξ values as shown in Fig. 13. Here T_{c1} is the superconducting critical temperature of lead metal or $Pb_{60}Bi_{40}$ alloy itself. The theoretically expected T_c/T_{c1} values for the aluminium-based alloys are zero in both the cases of $L = l/\xi = 1$ and 100 as plotted in Fig. 13, indicating that the superconducting state by the proximity effect is not obtainable for the present aluminium-based alloys due to the very small sizes of lead and lead–bismuth particles. Nevertheless, as summarized in Table I, the aluminium-based alloys exhibit a clear superconductivity, even though T_c is lower by about 13 to 42% than the highest values (7.19 and 8.9 K) of lead metal and lead–bismuth alloys. This is inconsistent with the expectation derived from the theory of the proximity effect. The inconsistency allows us to infer that the appearance of superconductivity for the present aluminium-based alloys is due not to the proximity effect of lead or lead-bismuth particles, but to the formation of superconducting circuits by a percolation mechanism. Although no clear evidence showing the distinct formation of the percolation path is obtained in the present work, the transmission electron micrographs shown in Figs 2, 3 and 5 reveal that (i) the lead and lead–bismuth particles are apt to precipitate along the grain boundaries, sub-boundaries and dislocations, and (ii) even within the matrix, their particles lie very finely and densely within a distance much shorter than the leak distance. The preferential precipitation of lead or lead–bismuth particles on such defects, and the highly dense distribution of the particles in the matrix, appear to enable the formation of superconducting circuits by the percolation mechanism along the tangled dislocations and sub-boundaries within the matrix and/or along the grain boundaries. Accordingly, the reason why the aluminium-based duplex alloys exhibited rather high T_c values in spite of the very small sizes of the dispersed particles is thought to originate from the formation of a superconducting percolation path along the dislocations, sub-boundaries and/or grain boundaries. Thus, the mechanism for the appearance of superconductivity for the aluminium-based crystalline alloys is speculated to be different from that for the nickel- [5] and copper- [6] based amorphous alloys, which have been interpreted to exhibit superconductivity due to the proximity effect of lead or lead–bismuth particles.

5. Summary

Aluminium-based duplex alloys exhibiting superconductivity were produced by melt-quenching the $Al_{100-x}Pb_x$, $(Al_{0.9}Si_{0.1})_{100-x}Pb_x$ and $(Al_{0.9}Si_{0.1})_{100-x}$-$(Pb_{0.6}Bi_{0.4})_x$ alloys containing immiscible lead and bismuth elements. The duplex alloys consisted of an aluminium matrix phase including fcc lead or hcp ε(Pb–Bi) particles. The particle size and the interparticle distance are ~10 to 40 nm and 40 to 100 nm, respectively, within the grains; ~65 nm and below ~30 nm at the grain boundaries for the lead phase; and ~15 to 60 nm and 30 to 60 nm within the grains for the ε(Pb–Bi) phase. The formation of the duplex alloys with finely dispersed lead or lead–bismuth particles was limited to less than 2 at % Pb for the Al–Pb system, about 5 at % Pb for the Al–Si–Pb system and about 5 at % (Pb + Bi) for the Al–Si–Pb–Bi system.

These duplex alloys were found to exhibit a superconductivity and the mechanism for the appearance of the superconductivity was interpreted as due to the formation of the percolation path along the highly tangled dislocations, sub-boundaries and/or grain boundaries, rather than the proximity effect of lead and lead–bismuth particles. The transition temperature, T_c, was 4.16 K for $Al_{98}Pb_2$, 3.94 K for $(Al_{0.9}Si_{0.1})_{95}Pb_5$ and 7.75 K for $(Al_{0.9}Si_{0.1})_{95}(Pb_{0.6}Bi_{0.4})_5$. The temperature gradient of the upper critical field near T_c and the upper critical field at 4.2 K are 0.075 T K^{-1} and 0.22 T for $(Al_{0.9}Si_{0.1})_{95}(Pb_{0.6}Bi_{0.4})_5$. Also, the critical current density, J_c, is 1.67 × 10^7 A m^{-2} at zero applied field and 4.2 K, and the maximum fluxoid pinning force is about 8.2 × 10^5 N m^{-3} at 4.2 K. Thus, the application of the melt-quenching technique to the aluminium-based alloys containing lead or lead plus bismuth elements, which are immiscible in an equilibrium state, was found to be very useful for the preparation of the superconducting duplex alloys consisting of aluminium-based phase including fine lead or lead–bismuth particles.

References

1. A. INOUE, M. OGUCHI, Y. HARAKAWA, K. MATSUZAKI, N. YANO and T. MASUMOTO, Japanese Patent Applications, Nos. 59-164693, 59-164694 and 59-164695 (1984).
2. A. INOUE, M. OGUCHI, K. MATSUZAKI, T. OGASHIWA and T. MASUMOTO, *Sci. Rep. Res. Inst. Tohoku Univ.* A-33 (1986) 111.

3. M. HANSEN, "Constitution of Binary Alloys", (McGraw-Hill, New York, 1958) pp. 245, 1028, 1084.
4. E. R. JETTE and E. B. GEBERT, *J. Chem. Phys.* **1** (1933) 735.
5. A. INOUE, M. OGUCHI, K. MATSUZAKI, Y. HARAKAWA and T. MASUMOTO, *J. Mater. Sci.* **21** (1986) 260.
6. A. INOUE, M. OGUCHI, K. MATSUZAKI and T. MASUMOTO, *Int. J. Rapid Solidification* **1** (1984–5) 273.
7. K. MATSUZAKI, A. INOUE, M. OGUCHI, N. TOYOTA and T. MASUMOTO *ibid.* in press.
8. W. B. PEARSON, Handbook of Lattice Spacings and Structures of Metals and Alloys (Pergamon, London, 1958) p. 124, 127.
9. H. JONES, *Aluminum* **54** (1978) 274.
10. D. SOLOMON and W. MORRIS, *Phil. Mag.* **11** (1931) 1090.
11. H. HOFE and H. HANEMANN, *Z. Metallkde.* **32** (1940) 112.
12. C. SURYANARAYANA and T. R. ANANTHARAMAN, *Solid State Commun.* **12** (1973) 87.
13. R. W. ROBERTS, Properties of Selected Superconductive Materials, NBS Technical Note 983, Supplement, (US Department of Commerce, Washington, 1978).
14. T. OTSUKA, Ferroelectrics and Superconductors, (Japan Institute of Metals, Sendai, 1973) p. 131.
15. C. KITTEL, Introduction to Solid State Physics, 5th edn. (John Wiley, New York, 1976) p. 154.
16. A. B. PIPPARD, *Proc. Roy. Soc. (Lond)* **A216** (1953) 547.
17. G. DEUTSCHER and D. G. de GENNES, Superconductivity, Vol. 2, edited by R. R. Parks (Marcel Dekker, New York, 1969) p. 1005.
18. W. SILVERT and A. SINGH, *Phys. Rev. Lett.* **28** (1972) 222.
19. M. LYON and G. ZEPP, *Can. J. Phys.* **55** (1977) 55.
20. W. SILVERT, *Solid State Commun.* **14** (1974) 635.
21. W. SILVERT and L. N. COOPER, *Phys. Rev.* **141** (1966) 336.

Received 23 December 1985
and accepted 6 May 1986